Frequency flicker of 2.3 GHz AlN-sapphire high-overtone bulk acoustic resonators

Rodolphe Boudot, Gilles Martin, Jean-Michel Friedt, and Enrico Rubiola

Citation: J. Appl. Phys. **120**, 224903 (2016); doi: 10.1063/1.4972102
View online: http://dx.doi.org/10.1063/1.4972102
View Table of Contents: http://aip.scitation.org/toc/jap/120/22
Published by the American Institute of Physics

JOURNAL OF APPLIED PHYSICS **120**, 224903 (2016)

Frequency flicker of 2.3 GHz AlN-sapphire high-overtone bulk acoustic resonators

Rodolphe Boudot, Gilles Martin, Jean-Michel Friedt, and Enrico Rubiola
FEMTO-ST, CNRS, UBFC, 26 chemin de l'Epitaphe, 25030 Besançon, Cedex, France

(Received 2 September 2016; accepted 29 November 2016; published online 15 December 2016)

We report the detailed characterization of 2.3 GHz AlN-Sapphire high-overtone bulk acoustic resonators (HBARs), with a typical loaded Q-factor of 25–30 $\times 10^3$, 15–20 dB insertion loss, and resonances separated by about 10 MHz. The temperature coefficient of frequency of HBARs is measured to be about -25 ppm/K. We observe at high-input microwave power a significant distortion of the HBAR resonance lineshape, attributed to non-linear effects. The power-induced fractional frequency variation of the HBAR resonance is measured to be about $-5 \times 10^{-10}/\mu$W. The residual phase noise of a HBAR is measured in the range of -110 to -130 dBrad^2/Hz at 1 Hz Fourier frequency, yielding resonator fractional frequency fluctuations at the level of -205 to -225 dB/Hz at 1 Hz and an ultimate HBAR-limited oscillator Allan deviation about 7×10^{-12} at 1 s integration time. The 1/*f* noise of the HBAR resonator is found to increase with the input microwave power. A HBAR resonator is used for the development of a low phase noise 2.3 GHz oscillator. An absolute phase noise of -60, -120, and -145 dBrad^2/Hz for offset frequencies of 10 Hz, 1 kHz, and 10 kHz, respectively, in excellent agreement with the Leeson effect, is measured. *Published by AIP Publishing*. [http://dx.doi.org/10.1063/1.4972102]

I. INTRODUCTION

Micromachined Bulk Acoustic Wave (BAW) resonators,[1,2] including thin-film bulk acoustic wave resonators (FBARs), solid-mounted resonators (SMRs) or high-overtone bulk acoustic resonators (HBARs), are well-adapted for the design and development of monolithically integrated, miniaturized and low-power consumption devices, high-Q filters, sensors or low-phase noise oscillators. Their low size, weight, and power (SWaP) properties make them of great interest for numerous industrial applications including telecommunication, sensing, radar signal processing, and defense systems. Billions of these components are spread each year around the world due to their specific functionalities and the maturity of their related technologies.

HBARs are known to provide at microwave frequency the highest Q-factor (Q) of any known acoustic resonator, demonstrating quality factor-frequency products up to 10^{14} (Refs. 1–3) and making them well-suited for the development of ultra-low phase noise oscillators.[4–6] A HBAR, which can be seen as an acoustic analogy to the optical Fabry-Perot interferometer, is obtained by stacking a thin piezoelectric transducer above a thick low-loss acoustic substrate. The piezoelectric film generates acoustic waves that propagate in the whole material stack. According to normal stress-free boundary conditions, stationary waves are obtained between top and bottom free surfaces. The complex electrical response of a HBAR presents a large spectrum envelope, induced by the thin film modes, modulated by the substrate discrete resonant modes whose repetition frequency f_s, inversely proportional to the round trip transit time in the substrate, is fixed by c_s/t_s where c_s is the wave acoustic velocity in the substrate and t_s is the substrate thickness.

The loaded Q-factor (Q_L) of the resonator, important figure of merit in low noise oscillator applications, is often measured as

$$Q_L = \frac{\nu_0}{\Delta\nu} \tag{1}$$

with ν_0, the resonant frequency and $\Delta\nu$, the resonance full-width at half maximum (FWHM) (-3 dB-linewidth). In a different approach, the same parameter can be measured as

$$Q_L = \frac{1}{2}\frac{d\varphi}{d\nu_0}\nu_0 \tag{2}$$

with $d\varphi/d\nu_0$, the resonator frequency discriminator-based phase-frequency slope. In this paper, we will name $Q_L|_{(1)}$ and $Q_L|_{(2)}$ the loaded Q-factor defined from Eqs. (1) and (2), respectively. Taking into account the resonator transmission S_{21} parameter at resonance, the unloaded Q-factor Q_0 can be defined from Q_L by[4]

$$\frac{Q_0}{Q_L} = \frac{1}{1 - 10^{S_{21}/20}}. \tag{3}$$

The spectral purity of an oscillator can be described from the measurement of the power spectral density (PSD), or phase noise spectral density $S_\varphi(f)$, of its phase fluctuations φ. The PSD of fractional frequency fluctuations $S_y(f)$ can be derived from $S_\varphi(f)$ by $S_y(f) = \frac{f^2}{\nu_0^2}S_\varphi(f)$ with f the Fourier offset frequency. In many cases, the frequency flicker of an oscillator, which appears as a $1/f^3$ line in the phase noise spectral density, and as a floor on the Allan deviation plot, originates from conversion of the amplifier phase flicker noise of the sustaining amplifier[7] into frequency flicker noise through the Leeson effect.[8,9] In some other specific cases, including state-of-the-art metrological BAW quartz crystal oscillators, it has been demonstrated that the fluctuation of the resonator natural frequency (resonator 1/*f* noise) can be the dominant effect.[10,11] The physical origin of the 1/*f* noise in resonators is still disputed but generally admitted to be related to the crystal phonons vibration.[12] Phonons, submitted to a high-level microwave signal, change the ultrasound propagation parameters of the crystal, making the resonant frequency fluctuate. More recently, the fluctuation dissipation theorem was used to evaluate the contribution of internal damping of thickness fluctuations to the level of noise for bulk acoustic wave cavities.[13]

In the presence of flicker, i.e., $S_\varphi(f) = b_{-1}/f$, the Allan deviation $\sigma_{yq}(\tau)$, stability of the resonator frequency, i.e., the time-domain stability of an oscillator in which the resonator is the only source of frequency instability, is given from

$$\sigma^2_{yq}(\tau) = \frac{2\ln(2)}{4Q_L^2} b_{-1}. \tag{4}$$

Different studies have focused on the flicker noise measurement of metrological HF quartz crystal resonators. In this domain, for instance, Rubiola *et al.* have reported phase noise measurements at the level of -131 dBrad^2/Hz at $f = 1$ Hz,[10] yielding, with $Q_L = 1.5 \times 10^6$, $\sigma_{yq}(\tau) \sim 1.1 \times 10^{-13}$ at 1 s integration time. At the opposite, until now, very few data have been published on the noise of MEMS BAW resonators. Bailey *et al.* have reported thick 640 MHz ZnO-YAG HBAR resonators, with $Q_L \sim 72\,000$, with exceptional $b_{-1} = -133$ dBrad^2/Hz, yielding $\sigma_{yq}(\tau) \sim 2 \times 10^{-12}$.[3] In Ref. 14, the FM noise of 2 GHz AlN-Sapphire HBAR resonators, with $Q_L \sim 20\,000$, was measured yielding $\sigma_{yq}(\tau)$ in the region of $1.1 - 3 \times 10^{-11}$. Gribaldo *et al.* reported residual 1/*f* noise of 2.3 GHz FBAR resonators, with $Q_L \sim 300$, such that $b_{-1} = -110$ to -125 dBrad^2/Hz, yielding $\sigma_{yq}(\tau)$ in the region of $1 - 6 \times 10^{-9}$.[15]

In this article, we investigate the residual 1/*f* noise of high-Q AlN-Sapphire 2.3 GHz HBAR resonators. In Section II, the architecture of HBAR resonators is presented and S-parameter characterization is reported. Careful attention is focused on the dependence of the HBAR resonance on temperature and input microwave power. In Section III, the resonator noise experimental setup and residual noise performances of resonators are reported. The impact of the carrier microwave power on the residual noise of the resonator is studied. In Section IV, a HBAR resonator is used as an ovenized frequency-control element towards the development of a low phase noise 2.3 GHz oscillator. Experimental results are found to be in excellent agreement with the Leeson effect.

II. HBAR RESONATOR DESCRIPTION

In the present study, two quasi-similar HBAR resonators, named HBAR1 and HBAR2, were studied. Figure 1(a) shows a schematic of these dual-port HBAR resonators. Their basic principle, detailed in Ref. 16, consists of coupling acoustic waves between two adjacent resonators, achieved by setting two resonators close to one another, allowing for evanescent waves between the resonator electrodes to overlap and hence to yield mode coupling conditions. This system exhibits two eigenmodes with slightly different eigenfrequencies: a symmetric mode in which the coupled resonators vibrate in phase and an anti-symmetric mode in which they vibrate in phase opposition. The bottom electrode is shared by the two resonators and is accessed through dedicated bias connected to ground. The HBAR substrate, made of sapphire, is 550 μm-thick, 1700 μm-wide, and 875 μm-long. The piezoelectric film, made of the AlN material, is 1 μm-thick. Figure 1(b) shows a photograph of the HBAR1 resonator before packaging. Following this step, the HBAR is enclosed in a duralumin box with output SMA connectors. Dedicated high-precision temperature electronics, inspired from Ref. 17, are used to stabilize the HBAR frequency at the mK level. This allows us to tune both resonators at about the same frequency.

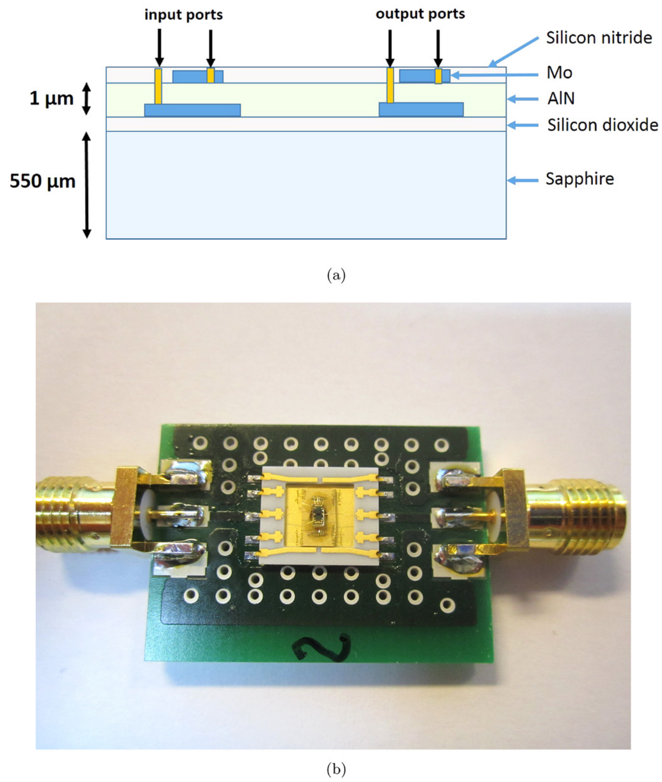

FIG. 1. (a) Schematic of a dual-port AlN-Sapphire HBAR resonator. (b) Photograph of the resonator HBAR1 before packaging.

We have investigated the HBAR resonator response versus the resonator temperature and the input microwave power. These measurements were performed using a vector network analyzer (VNA Agilent N5230A). Figure 2(a) shows the transmission parameter S_{21} for both resonators on a large span of 100 MHz. The frequency splitting between adjacent modes is about 10 MHz. Figure 2(b) shows a zoom on the studied mode at 2.3 GHz for both resonators. Both S_{12} and S_{21} transmission parameters are shown to highlight the correct symmetry of the resonator. For the resonator HBAR1, Q_L is 28 600 and insertion losses at resonance are about 16.0 dB. For the resonator HBAR2, Q_L is 25 600 and insertion losses at resonance are about 18.5 dB. The frequency splitting between both eigenmodes is about 124 kHz. Figure 2(c) shows the phase response in transmission for both resonators. Figure 2(d) shows reflexion

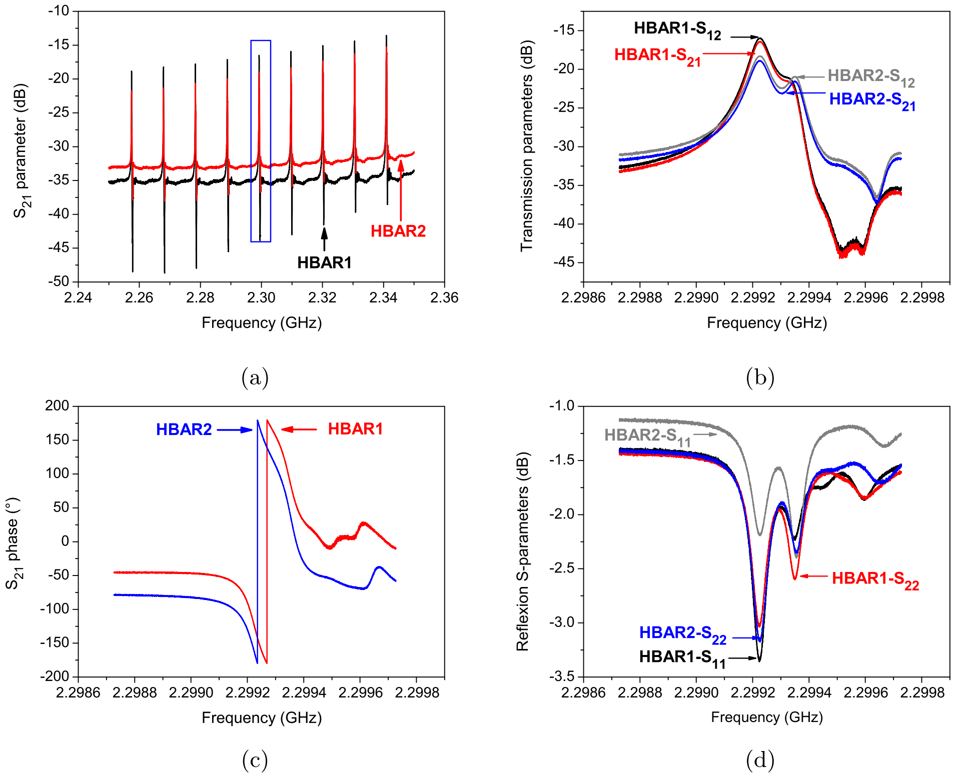

FIG. 2. S-parameters of both HBAR resonators. (a) S_{21} transmission parameters on a 100 MHz span. The rectangle indicates the studied mode. (b) S_{12} and S_{21} transmission parameters on a 1-MHz span. (c) Phase response in transmission (S_{21} parameter), (d) S_{11} and S_{22} reflexion parameters. The HBAR input power is −10 dBm.

parameters S_{11} and S_{22} for both resonators. These curves highlight the fact that input and output ports of these resonators are not-well 50Ω impedance-matched. For HBAR2, the port 2 impedance matching is better than for the port 1.

Figure 3 shows the resonance frequency versus temperature for HBAR1 and HBAR2. Experimental data are well-fitted by a linear function. The temperature coefficient of frequency (TCF) is measured to be −56.9 kHz/K (−24.7 ppm/K) for HBAR1 and −63.5 kHz/K (−27.6 ppm/K) for HBAR2. An effective permittivity calculation of stratified media[18] considering a 1-μm thick c-axis AlN film, sandwiched between two 100-nm thick Al electrodes, over a 500-μm c-plane sapphire substrate yields a temperature sensitivity of −28.5 ± 0.2 ppm/K, in correct agreement with the experiment. Figure 4 plots $Q_L|_{(1)}$ versus the temperature for both resonators HBAR1 and HBAR2. For both resonators, $Q_L|_{(1)}$ is found to increase slightly with temperature. We have also recorded the evolution of $Q_L|_{(2)}$ with temperature. The dependence on temperature of $Q_L|_{(2)}$ was found to be similar to the one of $Q_L|_{(1)}$. The value of $Q_L|_{(2)}$ was measured slightly higher than the value of $Q_L|_{(1)}$. We did not observe any variation of the resonator insertion losses (S_{21} parameter) between 40 and 95 °C. No variation of the reflexion parameter S_{11} was observed in this temperature range.

We have investigated experimentally the impact of the input microwave power on the HBAR resonator response using the VNA. For these tests, a microwave amplifier (Minicircuits ZX60–272LN-S+), with a gain of 15 dB, is placed at the direct output of the VNA port 1. The HBAR input port is connected to the amplifier output and the HBAR output port is directly connected to the VNA port 2. The VNA source power is tuned to change the microwave amplifier output power, i.e., the power at the HBAR input port, from −15 to 18 dBm. For these measurements, the HBAR

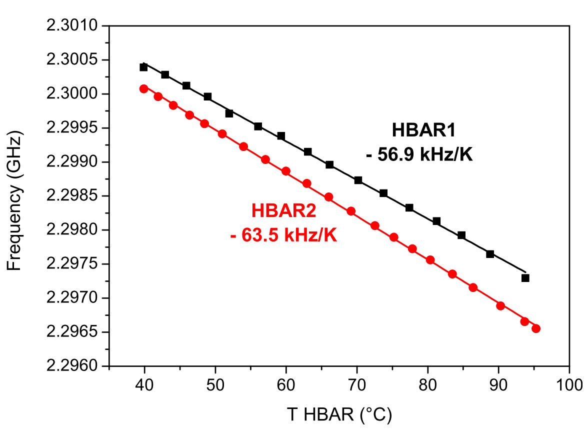

FIG. 3. Frequency of the resonators (HBAR1 and HBAR2) versus the resonator temperature. The HBAR input microwave power is −10 dBm.

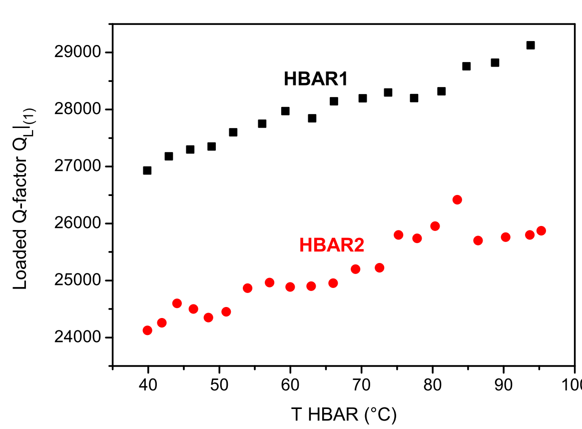

FIG. 4. Loaded Q-factor ($Q_L|_{(1)}$) of the resonators (HBAR1 and HBAR2) versus the resonator temperature. The input microwave power is −10 dBm.

resonator is temperature-stabilized. For several values of the HBAR input microwave power, the S_{21} parameter (magnitude and phase) and the S_{11} parameter (magnitude) are recorded on a frequency span of 150 kHz. For each new input microwave power value, a delay of about 3 min is taken before data recording to ensure a stable and stationary regime of the HBAR resonator thermal behavior. Figure 5 shows the HBAR1 resonance shape (S_{21} parameter) for different values of the HBAR input power. With increased input microwave power, we observe a clear and significant distortion of the resonance curve away from the Lorentzian line shape. This behavior is to our knowledge reported here for the first time in HBARs. Non linear, amplitude-frequency or isochronism effects have already been observed in quartz crystal resonators[19,20] and are known to depend on mechanical and energy trapping parameters. In our experiment, contrary to what is generally observed in quartz-crystal resonators,[19] the resonance shape is here more analogous to those induced by spring-softening Duffing non-linearity phenomena.[21–25] Such resonance shapes have already been reported in several types of MEMS or NEMS resonators, which due to their smaller size, can store less energy and are often driven into non-linear regimes at much lower excitation amplitudes than quartz crystal resonators. These properties have already been exploited to surpass fundamental limits of oscillators using nonlinear resonators[26] or amplifier noise evasion techniques in feedback loops.[27] Rigorous explanation would require here further theoretical investigations but this study remains out of the scope of this paper.

Figure 6 shows the HBAR resonance frequency versus the HBAR input microwave power for both HBARs. Experimental data are well-fitted by a linear function with a slope of -1350 Hz/mW ($-5.9 \times 10^{-10}/\mu$W in fractional value) for HBAR1 and -1060 Hz/mW ($-4.6 \times 10^{-10}/\mu$W in fractional value) for HBAR2. These values are close to typical amplitude-frequency coefficient values, of few 10^{-10} to some $10^{-9}/\mu$W, reported for quartz resonators.[10,20] We believe in the present study that the HBAR frequency variation is caused by the above-suggested non-linear effects and not by power-induced thermal heating of the HBAR resonator. For explanation, let's assume a very basic thermal model

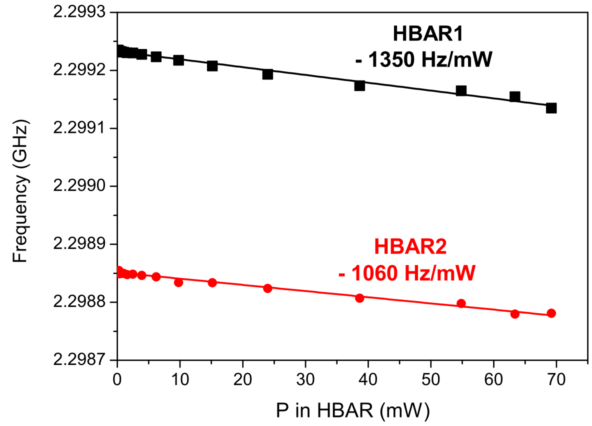

FIG. 6. Frequency of the resonators (HBAR1 and HBAR2) versus the HBAR microwave input power. The HBAR temperature is stabilized.

of the resonator HBAR1. The HBAR resonator substrate, 550 μm-thick, is made of a sapphire material with a thermal conductivity σ of about 25 W m^{-1} K^{-1}. This yields a thermal resistance R_{th}, described as $R_{th} = \frac{1}{\sigma}\frac{l}{S}$, with l, the unit length and S, the HBAR cross-section area, equal to 40 K/W. In our experiment, the total variation ΔP_{in} of the microwave power at the HBAR input is 70 mW. Only a fraction ($\sim$11%) of this power is actually absorbed by the resonator because of HBAR input port impedance mismatch (see $S_{11} \sim -1$ dB on Fig. 2(d) for HBAR2). Therefore, we estimate that the total variation of the input microwave power actually seen by the HBAR resonator is about 7.7 mW. From the R_{th} value and the HBAR TCF value of -63.5 kHz/°C, this power variation would induce a HBAR frequency variation of about -19.5 kHz whereas here, in Fig. 6, we measure a HBAR frequency variation of about -50 kHz, about 2.5 times bigger.

We have noted for each input microwave power value the loaded-Q_s $Q_L|_{(1)}$ and $Q_L|_{(2)}$. The corresponding results are reported in Fig. 7 for HBAR1. Q_L values are found to decrease slightly up to a few mW and found to rise again for higher microwave powers. The important point is to observe that for microwave powers higher than a few mW, both Q_L values diverge significantly. Both approaches (1) and (2) to define the loaded Q are often assumed to be equivalent, as derived from the elementary properties of the Lorentzian

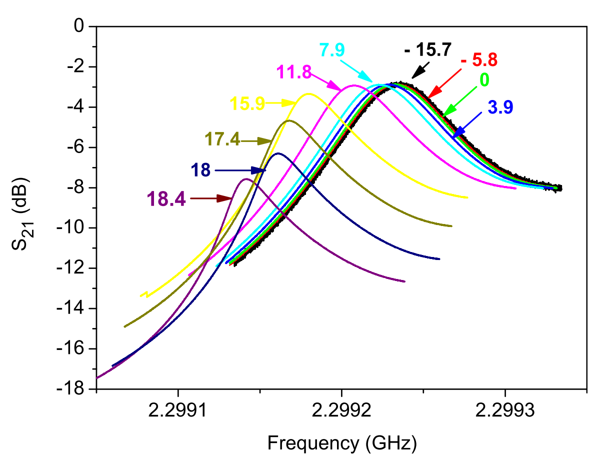

FIG. 5. HBAR1 resonance shape (S_{21} magnitude parameter) for several values of input microwave power (in dBm).

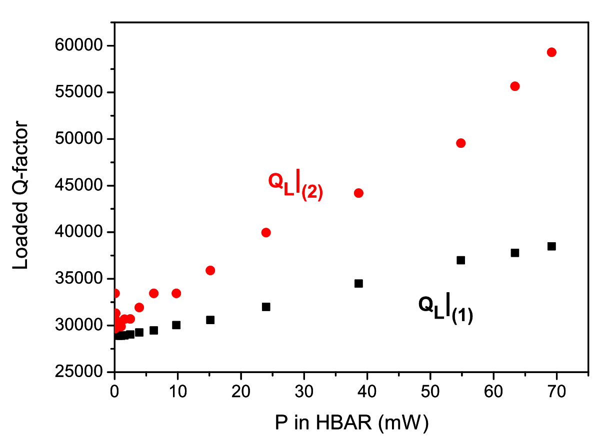

FIG. 7. Loaded Q-factor ($Q_L|_{(1)}$ and $Q_L|_{(2)}$) of HBAR1 versus the microwave input power. The HBAR temperature is stabilized.

line shape. However, in the presence of non-linearities, the resonance is warped, for (1) and (2) are no longer equivalent. One side of the line-shape is steeper than the other and $Q_L|_{(2)}$ gets larger than $Q_L|_{(1)}$, as reported in Ref. 21. It should be noticed that the Leeson effect,[8] which rules the oscillator stability as a consequence of the phase noise in the loop, relies on Eq. (2) and not on Eq. (1). For a microwave power of 17.5 dBm, we obtain $Q_L|_{(2)} = 60\,000$, yielding a $Q_L\nu_0$ product of 1.38×10^{14}. We note that we observed a rapid and significant degradation of the HBAR input port impedance matching for microwave powers higher than 45–50 mW. This degradation explains the increased insertion losses at high input power of the HBAR resonator shown in Fig. 5.

III. HBAR RESIDUAL NOISE MEASUREMENTS

Figure 8 describes the HBAR residual phase noise measurement setup principle. A 2.3 GHz frequency source (Keysight E8257D) is power-split into two arms. In the first arm, a HBAR resonator is implemented followed by a microwave amplifier to compensate for losses of the resonator. In the second arm a phase shifter is placed. Attenuators are placed in each arm to control the microwave power. Saturated by two signals of power of 5–10 dBm in quadrature with one another, a Schottky-diode double-balanced mixer (Minicircuits ZFM-4212+) works as a phase detector. The mixer output is low-pass filtered, amplified by a low-noise dc amplifier and sent into a fast Fourier transform (FFT) analyzer (HP3561A). The apparatus may employ a single HBAR in an unbalanced bridge arrangement as described above or two HBARs in a balanced bridge. The advantage of the single-HBAR measurement is its simplicity and to ensure that there is a single resonator contributing to the measured noise. Nevertheless, in this configuration, the frequency fluctuations of the source can be converted into phase fluctuations through the resonator. The higher the Q factor, the higher the contribution of the source noise to the overall output noise. In a balanced bridge system with 2 HBARs, the contribution of the synthesizer noise to the total output noise can be rejected. This assumes to be able to match the frequency of both HBARs (with temperature in our case) and to ensure to have identical loaded *Q*s (phase-versus-frequency slopes). A Q-mismatch within 10% warrants an oscillator noise rejection of 20 dB. Most of our measurements were performed in the single-resonator unbalanced bridge scheme. This method allowed us to detect the 1/*f* noise of HBARs for Fourier frequencies up to $f \sim 1$ kHz and HBAR driving powers down to about 5 dBm. For measurements of the HBAR noise under extended

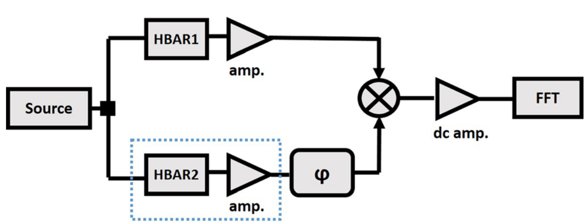

FIG. 8. HBAR resonator residual phase noise measurement setup. φ is a phase-shifter. A microwave mixer is used as a phase detector.

conditions, a dedicated phase noise setup inspired from Ref. 10, using carrier suppression techniques (to reduce the sustaining amplifier and mixer detection stage noise) and two resonators in a balanced bridge scheme (to reject the source frequency noise contribution), could be implemented. The sensitivity of the phase detector to amplitude noise (AM noise) can be reduced using the technique described in Ref. 28.

Figure 9 shows the PSD of phase fluctuations $S_\varphi(f)$ of the source (Keysight E8257D) at 2.3 GHz. The absolute phase noise of the source is −63, −102, −139, and −151 dBrad^2/Hz at $f = 1$, 100, 10^4, and 10^7 offset frequencies, respectively. Fractional frequency fluctuations of the source, described in terms of $S_y(f)$, are reported in Fig. 9 for additional information. In the resonator bandwidth, the equivalent phase noise $S_{\varphi s}(f)$ due to the source noise at the mixer input versus the resonator Q-factor can be written as

$$S_{\varphi s}(f) = 4Q_L^2 S_y(f) = 4Q_L^2 \frac{f^2}{\nu_0^2} S_\varphi(f). \tag{5}$$

Figure 10(a) shows the residual phase noise measurements of the resonator HBAR1 for several input microwave powers in a single-resonator unbalanced bridge. For information, the noise measurement setup floor (microwave amplifier + mixer + dc amplifier) and the calculated contribution of the source FM noise to the system output phase noise are plotted. For correct estimation of the latter contribution, it is important to note that Eq. (5) is no longer valid beyond the resonator bandwidth (∼40 kHz). Consequently, we measured the whole setup transfer function *H*(*f*). For this purpose, a random white noise generated by a FFT analyzer (HP3562A) source feeds the FFT input channel 1 and modulates the frequency of the 2.3 GHz source. The signal at the setup output is sent into the FFT analyzer (channel 2). The setup response was found to be well-approximated by a first-order low-pass filter transfer function, with a cutoff frequency of 41 kHz, signature of the HBAR resonator bandwidth. Thus, out of the resonator bandwidth, the source noise contribution is evaluated by multiplying $S_{\varphi s}(f)$ by *H*(*f*). For $f > 1$ kHz, the resonator noise measurement is mainly limited by the source noise contribution. In the 30–100 kHz range, the calculated source noise

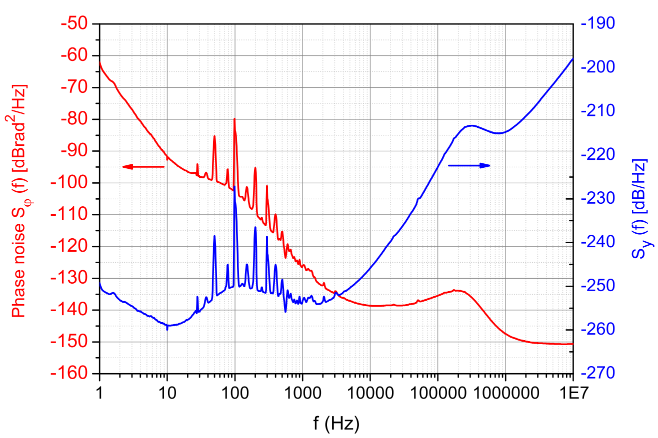

FIG. 9. Power spectral density of phase fluctuations and of fractional frequency fluctuations of the microwave synthesizer source (at 2.3 GHz).

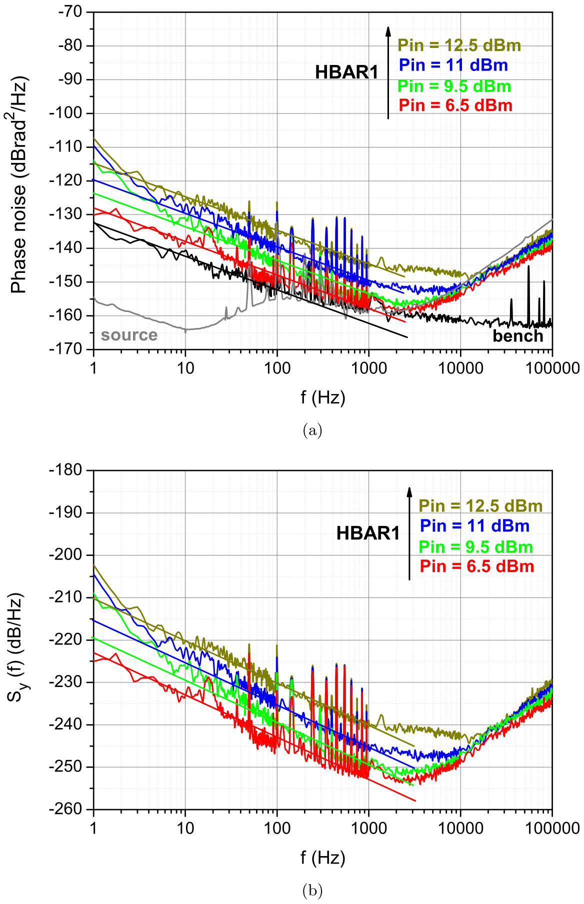

FIG. 10. Residual phase noise (a) and PSD of fractional frequency fluctuations of the resonator HBAR1 for several incident microwave power values. Solid lines are fitting curves with $1/f$ slopes. The residual noise of the measurement setup and calculated contribution of the source frequency noise are reported for information.

contribution does not fit perfectly and is found slightly (2–3 dB) higher than the measured noise. This behavior is still not explained and investigation is in progress. Anyway, this region has no impact on the estimation of the resonator frequency stability. The relative resonant frequency fluctuations of the resonator, proportional to the phase fluctuations divided by $4Q_L^2$, are reported in Fig. 10(b). We observe that the $1/f$ noise component of the HBAR resonator increases with increased input microwave power. This behavior has already been observed for quartz-crystal resonators[10] and FBAR resonators.[15] Residual phase noise in the range of -110 to -130 dBrad^2/Hz, yielding resonator fractional frequency fluctuations at the level of -205 to -225 dB/Hz, at 1 Hz Fourier frequency is measured. Similar results were obtained for the resonator HBAR2 with a slightly reduced dependence to input microwave power. For an additional test, in order to reject the contribution of the source FM noise, we did a resonator residual phase noise measurement by implementing a HBAR resonator in each arm of the noise measurement setup described in Fig. 8. Results, reported in Fig. 11 for an input microwave power of 9.5 dBm, are in correct agreement with measurements given in Fig. 10(a) for a single HBAR resonator. In this measurement, we observe a sudden decrease of noise after 30–40 kHz. Regarding the relative frequency deviation of the resonator as the input signal and the measured phase as the output, the resonator is equivalent to a low-pass filter characterized by the cutoff frequency $f_L = \nu_0/2Q_L \sim 40$ kHz. For $f > f_L$, the resonator filters its own frequency fluctuations, yielding an expected f^{-3} slope on the phase noise spectrum. This phenomenon was observed in various articles.[10,29] From these measurements, for $S_\varphi(f = 1\,\text{Hz}) = -130$ dBrad^2/Hz, the Allan deviation $\sigma_{yq}(\tau)$ given by Eq. (4) is calculated to be about 6.7×10^{-12} at 1 s integration time.

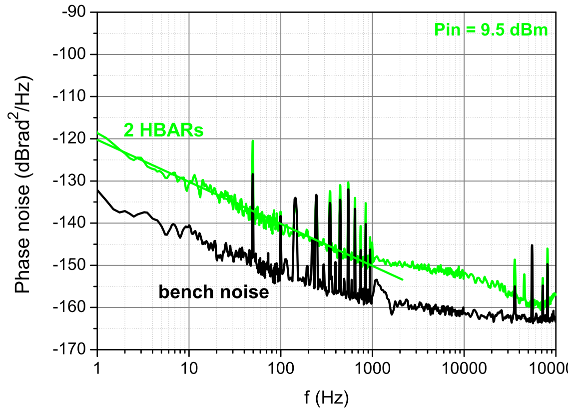

FIG. 11. Residual phase noise of a pair of HBAR resonators for a microwave input power of 9.5 dBm. The contribution of the source noise is largely rejected in this setup.

IV. HBAR-OSCILLATOR

We have developed a 2.3 GHz oscillator based on the resonator HBAR1. A schematic of the oscillator is given in Fig. 12. It combines in a circuit loop the resonator HBAR1, two sustaining amplifiers in serial configuration (Minicircuits ZX60–8000E-S+ and ZX60–6013 G-S+) with a total gain of about 25 dB, a microwave isolator, a coupler to extract the output signal, a phase shifter to adjust oscillation phase conditions, and a 100-MHz bandwidth surface acoustic wave (SAW) bandpass filter. A buffer output amplifier (Minicircuits ZX60–8000E-S+) is placed at the output of the coupler. The absolute phase noise of the 2.3 GHz output signal is measured using a signal source analyzer (Rohde-Schwarz FSWP). This instrument combines cross-correlation[30–32] and software defined radio techniques[33] for enhanced sensitivity. In the oscillator loop, the first amplifier input power is about -13 dBm, while the resonator input power is about 6 dBm.

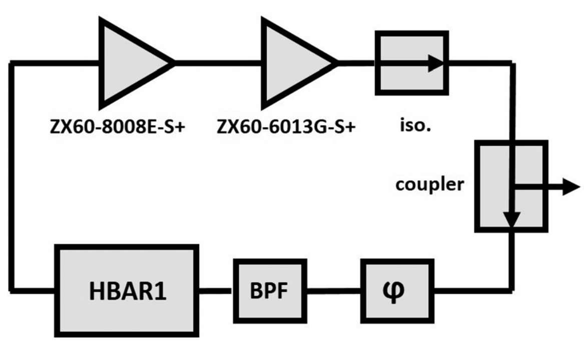

FIG. 12. Schematic of the 2.3 GHz HBAR-based (HBAR1) oscillator. BPF: bandpass filter. iso: isolator.

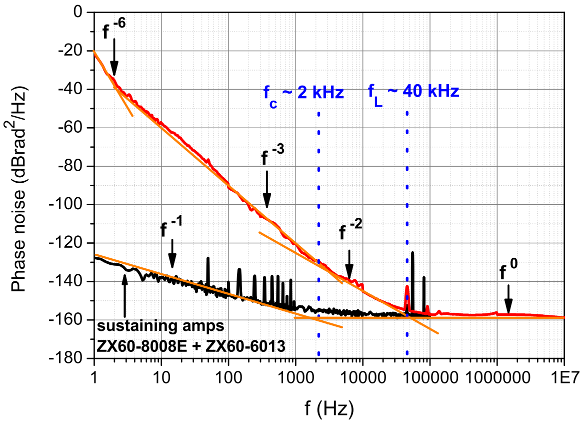

FIG. 13. Phase noise performances of the 2.3 GHz HBAR-oscillator. The residual phase noise of the sustaining amplifier stage, under identical input power conditions, is reported for information. Solid lines are fits to the different phase noise spectrum slopes. The oscillator phase noise is in excellent agreement with the Leeson effect.

Figure 13 shows the phase noise of the oscillator at 2.3 GHz. The residual phase noise of the sustaining amplifier stage is reported for information. The oscillator phase noise floor is in excellent agreement with the sustaining amplifier phase noise floor $S_{\varphi_0} = FkT/P_{in}$, where F is the amplifier noise figure, kT is the thermal energy, and P_{in} is the amplifier input power. Under our experimental conditions, it yields $S_{\varphi_0} = -159$ dBrad^2/Hz. For $f_c = 2$ kHz $< f < f = f_L = \nu_0/2Q_L \sim 40$ kHz, where f_L is the Leeson frequency and f_c is the amplifier cutoff frequency, the oscillator phase noise spectrum slope presents a f^{-2} slope, signature of a white frequency noise. For $f < f_c$, we obtain a frequency flicker region. In this region, phase noise performances of the oscillator are about 10 dB better than those reported in Ref. 6. This is mainly due to the use of sustaining amplifiers with lower $1/f$ noise. We claim and checked that phase noise performances in the 20 kHz–1 MHz range reported in Ref. 6 were limited by the phase noise measurement system (Agilent E5052B). For $f < 3$ Hz, the phase noise spectrum is well-fitted by a f^{-6} slope, signature of a frequency drift. For f > 20 kHz, phase noise performances of the present HBAR-oscillator are better than those of a state-of-the-art 100 MHz oven-controlled quartz crystal oscillator (OCXO) ideally frequency-multiplied to 2.3 GHz.[34]

V. CONCLUSIONS

We have reported the detailed characterization of 2.3 GHz AlN-Sapphire HBAR resonators with a loaded Q-factor of about 25 000 and TCFs of about -25 ppm/K. Distorted resonance lineshapes were observed for input microwave powers higher than 14–15 dBm, yielding amplitude-frequency effects at the level of $-5 \times 10^{-10}/\mu$W. Residual phase noise at the level of -110 to -130 dBrad^2/Hz at 1 Hz Fourier frequency was measured, yielding a resonator intrinsic frequency stability of about 7×10^{-12} at 1 s integration time. We observed that the $1/f$ noise of the resonator is increased with the microwave power. Similar behaviors were observed on two distinct resonators of similar architectures. We have constructed a 2.3 GHz HBAR-based oscillator. Phase noise performances of the source, in excellent agreement with conversion of the sustaining amplifier stage phase noise via the Leeson effect, are at the level of -120 and -145 dBrad^2/Hz at 1 and 10 kHz offset frequency, respectively.

ACKNOWLEDGMENTS

The authors would like to thank Vincent Giordano (FEMTO-ST) for fruitful discussions on resonator nonlinearities and phase noise measurements. The authors acknowledge David Rabus and Sébastien Alzuaga (FEMTO-ST) for HBAR TCF calculations. Cyrus Rocher (FEMTO-ST) has developed the electronic temperature controller used to stabilize the resonator temperature. Valérie Petrini (FEMTO-ST) helped to the device packaging. The authors thank A. Reinhardt and P. P. Lassagne (CEA-LETI) for supplying us the HBAR resonators.

This work has been supported by the Agence Nationale de la Recherche (ANR) Project Equipex Oscillator IMP. The Oscillator IMP Project funded in the frame of the French national Projets d'Investivement d'Avenir (PIA) targets at being a facility dedicated to the measurement of noise and short-term stability of oscillators and devices in the whole radio spectrum (from MHz to THz), including microwave photonics. This work has been partly supported by LabeX FIRST-TF.

[1]K. M. Lakin, G. R. Kline, and K. T. McCarron, IEEE Trans. Microwave Theory Tech. **41**, 2139 (1993).
[2]K. M. Lakin, IEEE Trans. Ultrason. Ferroelectr. Freq. Control **52**, 707 (2005).
[3]D. S. Bailey, M. M. Driscoll, R. Jelen, and B. R. McAvoy, IEEE Trans. Ultrason. Ferroelectr. Freq. Control **39**, 780 (1992).
[4]M. M. Driscoll, R. A. Jelen, and N. Matthews, IEEE Trans. Ultrason. Ferroelectr. Freq. Control **39**(6), 774 (1992).
[5]H. Yu, C. Lee, W. Pang, H. Zhang, A. Brannon, J. Kitching, and E. Sok Kim, IEEE Trans. Ultrason. Ferroelectr. Freq. Control **56**(2), 400 (2009).
[6]T. Daugey, J. M. Friedt, G. Martin, and R. Boudot, Rev. Sci. Instrum. **86**, 114703 (2015).
[7]R. Boudot and E. Rubiola, IEEE Trans. Ultrason. Ferrolectr. Freq. Control **59**(12), 2613 (2012).
[8]D. B. Leeson, Proc. IEEE **54**(2), 329 (1966).
[9]E. Rubiola, *Phase Noise and Frequency Stability in Oscillators* (Cambridge University Press, Cambridge, UK, 2008).
[10]E. Rubiola, J. Groslambert, M. Brunet, and V. Giordano, IEEE Trans. Ultrason. Ferroelectr. Freq. Control **47**(2), 361–368 (2000).
[11]E. Rubiola and V. Giordano, IEEE Trans. Ultrason. Ferroelectr. Freq. Control **54**(1), 15–22 (2007).
[12]F. L. Walls, P. H. Hendel, R. Besson, and J. J. Gagnepain, in Proceedings of the IEEE Frequency Control Symposium (1992), pp. 327–333.
[13]F. Stahl, M. Devel, J. Imbaud, R. Bourquin, and G. Cibiel, Appl. Phys. Lett. **107**, 103502 (2015).
[14]E. S. Ferre-Pikal, M. C. Delgado Aramburo, F. L. Walls, and K. M. Lakin, IEEE Trans. Ultrason. Ferroelectr. Freq. Control **48**(2), 506 (2001).
[15]S. Gribaldo, C. Chay, E. Tournier, and O. Llopis, IEEE Trans. Ultrason. Ferroelectr. Freq. Control **53**(11), 1982 (2006).
[16]A. Reinhardt, M. Delaye, J. Abergel, V. Kovacova, M. Allain, L. Andreutti, D. Mercier, J. Georges, F. Tomaso, and P. Lassagne, in *Proceedings of the IEEE International Ultrasonics Symposium* (IUS) (IEEE, 2013), pp. 1922–1925.
[17]R. Boudot, C. Rocher, N. Bazin, S. Galliou, and V. Giordano, Rev. Sci. Instrum. **76**, 095110 (2005).
[18]S. Ballandras, A. Reinhardt, V. Laude, A. Soufyane, S. Camou, W. Daniau, T. Pastureaud, W. Steichen, L. Raphael, M. Solal, and P. Ventura, J. Appl. Phys. **96**(12), 7731–7741 (2004).

[19]J. J. Gagnepain and R. Besson, "Nonlinear effects in piezoelectric quartz crystals," in *Physical Acoustics—Principles and Methods*, edited by W. P. Mason (Academic Press, New York, NY, 1975), Vol. XII, pp. 245–288.
[20]N. Gufflet, R. Bourquin, and J. J. Boy, "Isochronism defect for various doubly rotated cut quartz resonators," IEEE Trans. Ultrason. Ferrolectr. Freq. Control **49**(4), 514–518 (2002).
[21]A. H. Nayfeh and D. T. Mook, *Nonlinear Oscillations* (Wiley, 1995), Figure 1.5, p. 9.
[22]S. Lee and C. T. C. Nguyen, in Proceedings of the 2003 International Frequency Control Symposium and PDA Exhibition Jointly With the 17th European Frequency Time Forum (2003), pp. 341–349.
[23]R. M. C. Mestrom, R. H. B. Fey, and H. Nijmejer, IEEE/ASME Trans. Mechatron. **14**(4), 423 (2009).
[24]D. K. Agrawal and A. A. Seshia, IEEE Trans. Ultrason. Ferrolectr. Freq. Control **61**(12), 1938–1951 (2014).
[25]I. Kovacic and M. J. Brennan, *The Duffing Equation: Nonlinear Oscillators and Their Behaviour* (Wiley, 2011).
[26]L. G. Villanueva, E. Kenig, R. B. Karabalin, M. H. Matheny, R. Lifshitz, M. C. Cross, and M. L. Roukes, Phys. Rev. Lett. **110**, 177208 (2013).
[27]B. Yurke, D. S. Greywall, A. N. Pargellis, and P. A. Busch, Phys. Rev. A **51**, 4211 (1995).
[28]G. Cibiel, M. Regis, E. Tournier, and O. Llopis, IEEE Trans. Ultrason. Ferroelectr. Freq. Control **49**(6), 784 (2002).
[29]J. J. Gagnepain, "Fundamental noise studies of quartz crystal resonators," in Proceedings of the 30th Frequency Control Symposium, Atlantic City, NJ, 1976, pp. 84–91.
[30]E. Rubiola and V. Giordano, Rev. Sci. Instrum. **73**, 2445 (2002).
[31]E. Rubiola and R. Boudot, IEEE Trans. Ultrason. Ferrolectr. Freq. Control **54**(5), 926 (2007).
[32]C. W. Nelson, A. Hati, and D. Howe, Rev. Sci. Instrum. **85**, 024705 (2014).
[33]J. A. Sherman and R. Jordens, Rev. Sci. Instrum. **87**, 054711 (2016).
[34]B. François, C. E. Calosso, M. Abdel Hafiz, S. Micalizio, and R. Boudot, Rev. Sci. Instrum. **86**, 094707 (2015).